Atmos. Chem. Phys., 16, 10351–10368, 2016
www.atmos-chem-phys.net/16/10351/2016/
doi:10.5194/acp-16-10351-2016

Atmospheric Chemistry and Physics Open Access EGU

An evaluation of IASI-NH_3 with ground-based Fourier transform infrared spectroscopy measurements

Enrico Dammers[1], Mathias Palm[2], Martin Van Damme[1,3], Corinne Vigouroux[4], Dan Smale[5], Stephanie Conway[6], Geoffrey C. Toon[7], Nicholas Jones[8], Eric Nussbaumer[9], Thorsten Warneke[2], Christof Petri[2], Lieven Clarisse[3], Cathy Clerbaux[3], Christian Hermans[4], Erik Lutsch[6], Kim Strong[6], James W. Hannigan[9], Hideaki Nakajima[10], Isamu Morino[11], Beatriz Herrera[12], Wolfgang Stremme[12], Michel Grutter[12], Martijn Schaap[13], Roy J. Wichink Kruit[14], Justus Notholt[2], Pierre-F. Coheur[3], and Jan Willem Erisman[1,15]

[1]Cluster Earth and Climate, Department of Earth Sciences, Vrije Universiteit Amsterdam, Amsterdam, the Netherlands
[2]Institut für Umweltphysik, University of Bremen, Bremen, Germany
[3]Spectroscopie de l'Atmosphère, Service de Chimie Quantique et Photophysique, Université Libre de Bruxelles (ULB), Brussels, Belgium
[4]Royal Belgian Institute for Space Aeronomy (BIRA-IASB), Brussels, Belgium
[5]National Institute of Water and Atmosphere, Lauder, New Zealand
[6]University of Toronto, Toronto, Ontario, Canada
[7]Jet Propulsion Laboratory, California Institute of Technology, Pasadena, California USA
[8]Centre for Atmospheric Chemistry, University of Wollongong, Wollongong, Australia
[9]NCAR, Boulder, Colorado, USA
[10]Atmospheric Environment Division, National Institute for Environmental Studies (NIES), Tsukuba, Japan
[11]National Institute for Environmental Studies, 16-2 Onogawa, Tsukuba, Ibaraki, 305-8506, Japan
[12]Centro de Ciencias de la Atmósfera, Universidad Nacional Autonoma de Mexico, Mexico City, Mexico
[13]TNO Built Environment and Geosciences, Department of Air Quality and Climate, Utrecht, the Netherlands
[14]National Institute for Public Health and the Environment (RIVM), Bilthoven, the Netherlands
[15]Louis Bolk Institute, Driebergen, the Netherlands

Correspondence to: Enrico Dammers (e.dammers@vu.nl)

Received: 15 February 2016 – Published in Atmos. Chem. Phys. Discuss.: 15 March 2016
Revised: 18 July 2016 – Accepted: 19 July 2016 – Published: 16 August 2016

Abstract. Global distributions of atmospheric ammonia (NH_3) measured with satellite instruments such as the Infrared Atmospheric Sounding Interferometer (IASI) contain valuable information on NH_3 concentrations and variability in regions not yet covered by ground-based instruments. Due to their large spatial coverage and (bi-)daily overpasses, the satellite observations have the potential to increase our knowledge of the distribution of NH_3 emissions and associated seasonal cycles. However the observations remain poorly validated, with only a handful of available studies often using only surface measurements without any vertical information. In this study, we present the first validation of the IASI-NH_3 product using ground-based Fourier transform infrared spectroscopy (FTIR) observations. Using a recently developed consistent retrieval strategy, NH_3 concentration profiles have been retrieved using observations from nine Network for the Detection of Atmospheric Composition Change (NDACC) stations around the world between 2008 and 2015. We demonstrate the importance of strict spatio-temporal collocation criteria for the comparison. Large differences in the regression results are observed for changing intervals of spatial criteria, mostly due to terrain characteristics and the short lifetime of NH_3 in the atmosphere. The seasonal variations of both datasets are consistent for most sites. Correlations are found to be high at sites in areas with considerable NH_3 levels, whereas correlations are lower at sites with low atmospheric NH_3 levels close to the detection limit of the IASI instrument. A combination of the observations

from all sites ($N_{obs} = 547$) give a mean relative difference of $-32.4 \pm (56.3)$ %, a correlation r of 0.8 with a slope of 0.73. These results give an improved estimate of the IASI-NH3 product performance compared to the previous upper-bound estimates (-50 to $+100$ %).

1 Introduction

Humankind has increased the global emissions of reactive nitrogen to an unprecedented level (Holland et al., 1999; Rockström et al., 2009). The current global emissions of reactive nitrogen are estimated to be a factor of 4 larger than pre-industrial levels (Fowler et al., 2013). Consequently, atmospheric deposition of reactive nitrogen to ecosystems has substantially increased as well (Rodhe et al., 2002; Dentener et al., 2006). Ammonia (NH_3) emissions play a major role in this deposition with a total emission of 49.3 Tg in 2008 (Emission Database for Global Atmospheric Research (EDGAR), 2011). Although NH_3 emissions are predominantly from agriculture in the Northern Hemisphere, wildfires also play a role, with biomass burning contributing up to 8 % of the global emission budget (Sutton et al., 2013). NH_3 has been shown to be a major factor in the acidification and eutrophication of soil and water bodies, which threatens biodiversity in vulnerable ecosystems (Bobbink et al., 2010; Erisman et al., 2008, 2011). Through reactions with sulfuric and nitric acid, NH_3 also contributes to the formation of particulate matter, which is associated with adverse health effects (Pope III et al., 2009). Particulate ammonium salts contribute largely to aerosol loads over continental regions (Schaap et al., 2004). Through its role in aerosol formation, NH_3 also has an impact on global climate change as hygroscopic ammonium salts are of importance for the aerosol climate effect and thus the global radiance budget (Adams et al., 2001). Furthermore increased NH_3 concentrations in the soil also enhance the emission of nitrous oxide (N_2O), which is an important greenhouse gas and an ozone-depleting substance (Ravishankara et al., 2009). Finally nitrogen availability is a key factor for the fixation of carbon dioxide (CO_2) and thus it is an important factor in climate change.

Despite the fact that NH_3 at its current levels is a major threat to the environment and human health, relatively little is known about its total budget and global distribution (Sutton et al., 2013; Erisman et al., 2007). Surface observations are sparse and mainly available for northwestern Europe, the United States, and China (Van Damme et al., 2015a). At the available sites, in situ measurements are mostly performed with relatively poor temporal resolution due to the high costs of performing reliable NH_3 measurements with high temporal resolution. These measurements of NH_3 are also hampered by sampling artefacts caused by the reactivity of NH_3 and the evaporation of ammonium nitrate (Slanina et al., 2001; von Bobrutzki et al., 2010; Puchalski et al., 2011). As the lifetime of atmospheric NH_3 is rather short, on the order of hours to a few days, due to efficient deposition and fast conversion to particulate matter, the existing surface measurements are not sufficient to estimate global emissions without inducing large errors. The lack of vertical profile information further hampers the quantification of the budget, with only a few reported airborne measurements (Nowak et al., 2007, 2010; Leen et al., 2013; Whitburn et al., 2015).

Advanced IR sounders such as the Infrared Atmospheric Sounding Interferometer (IASI), the Tropospheric Emission Spectrometer (TES), and the Cross-track Infrared Sounder (CrIS) enable retrievals of atmospheric NH_3 (Beer et al., 2008; Coheur et al., 2009; Clarisse et al., 2009; Shephard et al., 2011; Shephard and Cady-Pereira, 2015). The availability of satellite retrievals provides a means to consistently monitor global NH_3 distributions. Global distributions derived from IASI and TES observations have shown high NH_3 levels in regions not covered by ground-based data. In this way, more insight was gained into known and unknown NH_3 sources worldwide including biomass burning, industry, and agricultural areas. Hence, satellite observations have the potential to improve our knowledge of the distribution of global emissions and their seasonal variation due to their large spatial coverage and (bi-)daily observations (Zhu et al., 2013; Van Damme et al., 2014a, 2015b; Whitburn et al., 2015; Luo et al., 2015). However, the satellite observations remain poorly validated with only a few dedicated campaigns performed with limited spatial, vertical, or temporal coverage (Van Damme et al., 2015a; Shephard et al., 2015; Sun et al., 2015).

Only a few studies have explored the quality of the IASI-NH_3 product. A first evaluation of the IASI observations was made over Europe using the LOTOS-EUROS model and has shown the respective consistency of the measurements and simulations (Van Damme et al., 2014b). A first comparison using ground-based and airborne measurements to validate the IASI-NH_3 dataset was made in Van Damme et al. (2015a). They confirmed consistency between the IASI-NH_3 dataset and the available ground-based observations and showed promising results for validation by using independent airborne data from the CalNex campaign. Nevertheless, that study was limited by the availability of independent measurements and suffered from representativeness issues for the satellite observations when comparing to surface concentration measurements. One of the key conclusions was the need for vertical profiles (e.g. ground-based remote sensing products or upper-air in situ measurements to compare similar quantities). Recently, Dammers et al. (2015) developed a retrieval methodology for Fourier transform infrared spectroscopy (FTIR) instruments to obtain remotely sensed measurements of NH_3 and demonstrated the retrieval characteristics for four sites located in agricultural and remote areas. Here we explore the use of NH_3 total columns obtained with ground-based FTIR at nine stations with a range of NH_3 pol-

lution levels to validate the IASI-NH_3 satellite product by Van Damme et al. (2014a).

First, we concisely describe the ground-based FTIR retrieval and IASI-NH_3 product datasets in Sects. 2.1 and 2.2. Next we describe the methodology of the comparison in Sect. 2.3 followed by the presentation of the results in Sect. 3, which are then summarized and discussed in Sect. 4.

2 Description of the satellite and FTIR datasets and validation methodology

2.1 IASI-NH_3 product

The first global NH_3 distribution was obtained by a conventional retrieval method applied to IASI spectra (Clarisse et al., 2009), followed by an in-depth case study, using a more sophisticated algorithm, of the sounder's capabilities depending on the thermal contrast (defined in Van Damme et al., 2014a, as the temperature differences between the Earth surface and the atmosphere at 1.5 km altitude; Clarisse et al., 2010). In this study we use the NH_3 product developed by Van Damme et al. (2014a). Their product is based on the calculation of a dimensionless spectral index (hyperspectral range index: HRI), which is a quantity representative of the amount of NH_3 in the total atmospheric column. This HRI is then converted into NH_3 total columns using look-up tables based on numerous forward simulations for various atmospheric conditions. These look-up tables relate the HRI and the thermal contrast to a total column of NH_3 (Van Damme et al., 2014a). The product includes an error characterization of the retrieved column based on errors in the thermal contrast and HRI. Important advantages of this method over the method by Clarisse et al. (2009) are the relatively small computational cost, the improved detection limit, and the ability to identify smaller emission sources and transport patterns above the sea. One of the limitations of this method is the use of only two NH_3 vertical profiles: a "source profile" for land cases and a "transported profile" for sea cases (illustrated in Van Damme et al., 2014a, Fig. 3). Another limitation of the product is that it does not allow the calculation of an averaging kernel to account for the vertical sensitivity of the instrument sounding to different layers in the atmosphere. In this paper we will use NH_3 total columns retrieved from the IASI-A instrument (aboard of the MetOp-A platform) morning overpass (AM) observations (i.e. 09:30 local time at the Equator during overpass), which have a circular footprint of 12 km diameter at nadir and an ellipsoid shaped footprint of up to 20 km × 39 km at the outermost angles. We will use observations from 1 January 2008 to 31 December 2014. Figure 1 shows the mean IASI-NH_3 total column distribution (all observations gridded to a $0.1^\circ \times 0.1^\circ$ grid) using observations above land for the years 2008–2014. The mean columns are obtained through a weighting with the relative error (see Van Damme et al., 2014a). The bottom left inset shows the corresponding relative error.

2.2 FTIR-NH_3 retrieval

The FTIR-NH_3 retrieval methodology used here is described in detail in Dammers et al. (2015), and a summary is given here. The retrieval is based on the use of two spectral microwindows, which contain strong individual NH_3 absorption lines. The two spectral windows [930.32–931.32 cm^{-1}, MW1] and [962.70–970.00 cm^{-1}, MW2] or the wider versions for regions with very low concentrations [929.40–931.40 cm^{-1}, MW1 Wide] and [962.10–970.00 cm^{-1}, MW2 Wide] are fitted using SFIT4 (Pougatchev et al., 1995; Hase et al., 2004, 2006) or a similar retrieval algorithm (Hase et al., 1999) based on the optimal estimation method (Rodgers, 2000) to retrieve the volume mixing ratios (in ppbv) and total columns of NH_3 (in molecules cm^{-2}). Major interfering species in these windows include H_2O, CO_2, and O_3. Minor interfering species are N_2O, HNO_3, CFC-12, and SF_6. For the line spectroscopy, the HITRAN 2012 (Rothman et al., 2013) database is used with a few adjustments for CO_2 (ATMOS, Brown et al., 1996), and sets of pseudo-lines generated by NASA-JPL (G. C. Toon) are used for the broad absorptions by heavy molecules (i.e. CFC-12, SF_6). The a priori profiles of NH_3 are based on balloon measurements (Toon et al., 1999) and scaled to fit common surface concentrations at each of the sites. An exception is made for the a priori profile at Réunion Island, where a modelled profile from the MOZART model is used (Louisa Emmons, personal communication, 2014). There, the profile peaks at a height of 4–5 km, as NH_3 is expected to be due to transport of biomass burning emissions on Réunion Island and Madagascar. For all stations, the a priori profiles for interfering species are taken from the Whole Atmosphere Community Climate Model (WACCM, Chang et al., 2008). Errors in the retrieval are typically $\sim 30\,\%$ (Dammers et al., 2015), which are mostly due to uncertainties in the spectroscopy in the line intensities of NH_3 and the temperature and pressure broadening coefficients (HITRAN 2012).

An effort has been made to gather observations from most of the station part of the Network for the Detection of Atmospheric Composition Change (NDACC), which have obtained relevant solar spectra between 1 January 2008 and 31 December 2014. We excluded stations which have only retrieved or are believed to have NH_3 total columns smaller than 5×10^{15} (molecules cm^{-2}) during the study interval (i.e. Arctic and Antarctic and other stations with concentrations below the expected limits of the IASI-NH_3 product, at best $\sim 5 \times 10^{15}$ for observations with high thermal contrast). Figure 1 shows the positions of the FTIR stations used in this study. The retrieved NH_3 total columns (molecules cm^{-2}) for each of the stations are shown in Fig. 2. The number of available observations per station varies as does the range in total columns with high val-

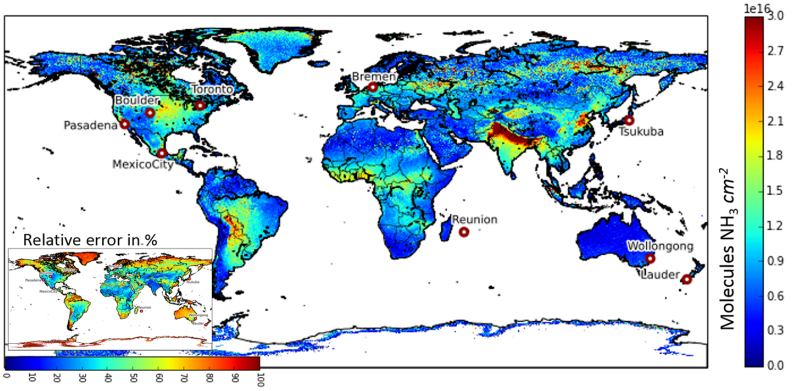

Figure 1. Mean IASI-NH_3 total column distribution for the period between January 2008 and January 2015. The total columns are a weighted average of the individual observations weighted with the relative error. Red circles indicate the positions of the FTIR stations.

ues of $\sim 100 \times 10^{15}$ (molecules cm^{-2}) observed at Bremen and low values of about 1×10^{15} (molecules cm^{-2}) at Saint Denis, Réunion. The following provides a short description of each of the sites used in this study and retrieved NH_3 columns (molecules cm^{-2}). Additionally, a short summary can be found in Table 1.

The Bremen site was operated on the university campus by the University of Bremen in the northern part of the city (Velazco et al., 2007). Bremen is located in the northwest of Germany, which is characterized by intensive agriculture. It is most suitable for comparisons with IASI given the very high observed concentrations (Fig. 2, blue) and flat geography surrounding the station. NH_3 sources near the measurement station include manure application to fields, livestock housing, and exhaust emissions of local traffic. The retrieved NH_3 total columns peak in spring due to manure application and show an increase in summer due to increased volatilization of NH_3 from livestock housing and fields when temperatures increase during summer.

The Toronto site (Wiacek et al., 2007) is located on the campus of the University of Toronto, Canada. The city is next to Lake Ontario with few sources to the south. NH_3 sources are mainly due to agriculture as well as local traffic in the city. Occasionally, NH_3 in smoke plumes from major boreal fires to the north and west of the city can be observed (Lutsch et al., 2016). The retrieved columns (Fig. 2, green) show increased values during summers as well as peaks in spring.

The Boulder observation site is located at the NCAR Foothills Lab in Boulder, Colorado, United States of America, about 60 km northwest of the large metropolitan Denver area. It is located at 1.6 km a.s.l. on the generally dry Colorado Plateau. Directly to the west are the foothills of the Rocky Mountains and to the east are rural grasslands, as well as farming and ranching facilities. Among them are large cattle feed lots to the northeast near Greeley approximately 90 km away. The area is subject to occasional seasonal local forest fires and also occasionally sees plumes from fires as distant as Washington or California. The retrieved columns (Fig. 2, grey) show the largest increase during summers.

The Tsukuba site (Ohyama et al., 2009) is located at the National Institute for Environmental Studies (NIES) in Japan. The region is a mixture of residential and rural zones with mountains to the north. NH_3 sources near the measurement site include manure and fertilizer applications and exhaust emissions of local traffic in the surrounding city with a large part originating from the Tokyo metropolitan area. The retrieved columns (Fig. 2, red) show a general increase during the summers due to increased volatilization rates.

The Pasadena site lies on the northern edge of the Los Angeles conurbation in the United States of America, at the foot of the San Gabriel Mountains which rise steeply to the north to over 1.5 km altitude within 5 km distance. Local sources of NH_3 include traffic, livestock, and occasional fires. FTIR observations typically take place around local noon to avoid solar obstruction by nearby buildings and morning stratus clouds, which are common in May–July. The highest retrieved columns (Fig. 2, cyan) are observed during the summers.

The Mexico City site is located on the campus of the National Autonomous University of Mexico (UNAM) at 2280 m a.s.l., south of the metropolitan area. Surface NH_3 concentrations were measured by active open-path FTIR during 2003 with typical values between 10 and 40 ppb (Moya et al., 2007). The megacity is host to more than 22 million inhabitants, over 5 million motor vehicles, and a wide variety of industrial activities. Low ventilation during night and morning causes an effective accumulation of the NH_3 and other pollutants in Mexico City, which is located in a flat basin surrounded by mountains. The concentration and vertical distribution of pollutants are dominated by the large emissions and the dynamics of the boundary layer, which is on average 1.5 km height during the IASI morning overpass (Stremme et al., 2009, 2013). The retrieved columns (Fig. 2,

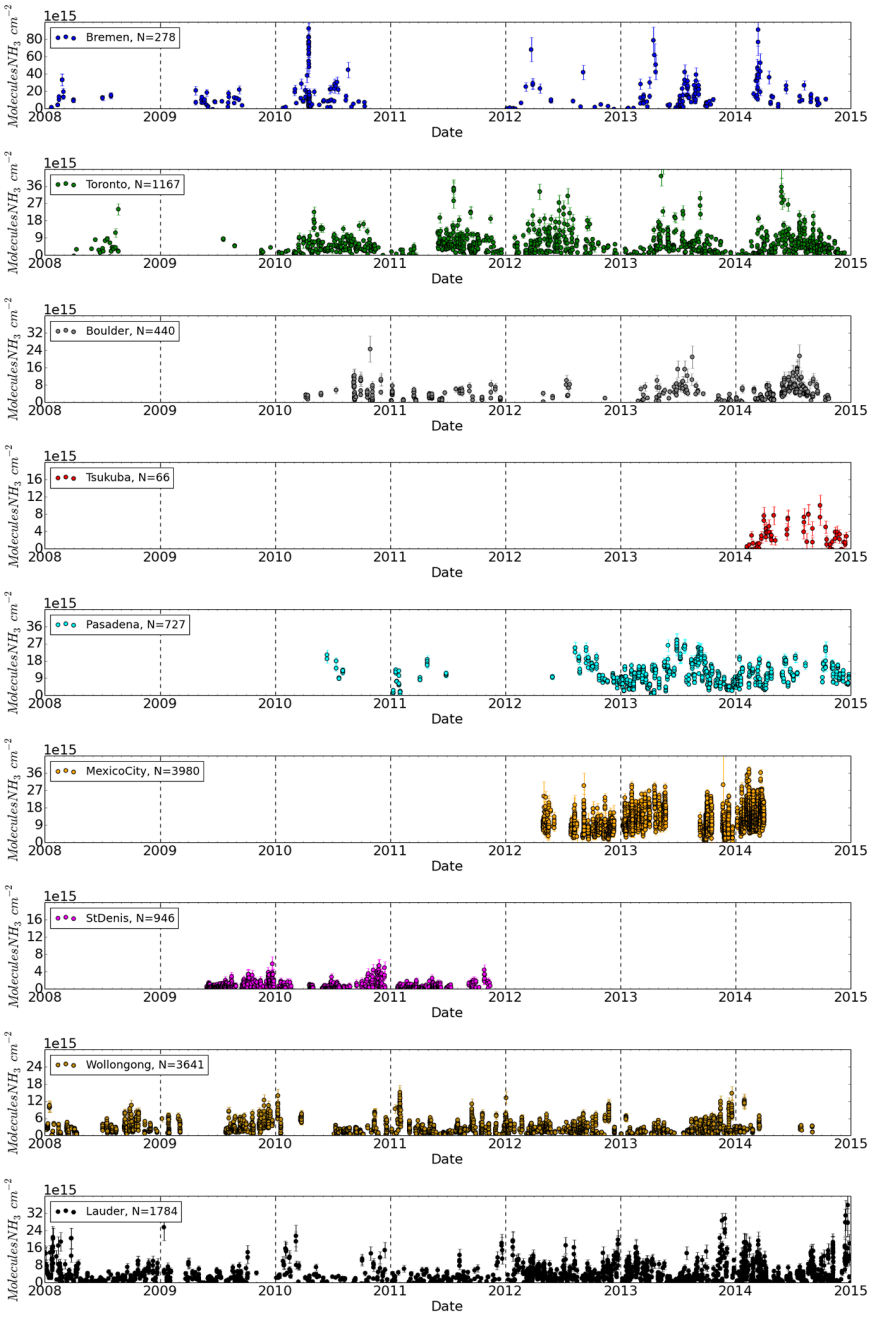

Figure 2. FTIR-retrieved NH_3 total columns (in molecules cm^{-2}). Note that the labels on the vertical axis vary for each site.

orange) show an increase during the summers as well as a large daily variation.

The measurement site on the university campus of Saint Denis (Senten et al., 2008) is located on the remote Réunion Island in the Indian Ocean. Observed NH_3 columns (Fig. 2, purple) are usually low due to the lack of major sources near the site, but increases are observed during the fire season (September–November) with possible fire plumes originating from Madagascar, as already observed in another study involving short-lived species (Vigouroux et al., 2009). Local NH_3 emissions include fertilizer applied for sugar cane production and local biomass burning.

The Wollongong site is located on the campus of the University of Wollongong. The city of Wollongong is on the southeast coast of Australia with the university only about 2.5 km from the ocean. The measurement site is also influenced by a 400 m escarpment 1 km to the west and the city of Sydney 60 km to the north. NH_3 sources come mainly

from city traffic, as well as seasonal forest fires that can produce locally high amounts of smoke and subsequent NH_3 emissions (Paton-Walsh et al., 2005). The retrieved columns (Fig. 2, brown) peak during the summer season due to the higher temperatures and seasonal forest fires.

The Lauder (Morgenstern et al., 2012) National Institute of Water and Atmospheric Research (NIWA) station in Central Otago, New Zealand, is located in a hilly region with NH_3 emissions in the valley surrounding the station mostly due to livestock grazing and fertilizer application. The observed columns (Fig. 2, black) show a general increase during summers due to increased volatilization rates.

2.3 FTIR and satellite comparison methodology

2.3.1 Co-location and data criteria

NH_3 is highly variable in time and space, which complicates the comparison between the IASI and FTIR observations. Therefore collocation criteria were developed to investigate and mitigate the effect of the spatial and temporal differences between the FTIR and IASI observations on their correlation. So far, there is no model to describe the representativeness of a site for the region so a simple criterion was initially derived by analysing the terrain around each site and comparing the correlation of the IASI and FTIR observations for multiple time and spatial differences to find the best correlation. To illustrate the differences between the representativeness of the sites we take the stations at Bremen, Lauder, and Wollongong as examples. Around Bremen the terrain is flat with high reported NH_3 emissions (Kuenen et al., 2014) in the region surrounding the city. In contrast, Lauder is located in a hilly region with low NH_3 emissions mostly due to local livestock grazing and fertilizer application in the surrounding valleys (EDGAR, 2011). Owing to the flat terrain, the region around Bremen should, in principle, have more homogeneous concentrations than Lauder. A more extreme case for geographical inhomogeneity is Wollongong. Wollongong is located at the coast near a 400 m escarpment without major nearby NH_3 sources. Hence increasing distances between the satellite measurement pixel centre and the station may negatively impact the comparison due to the short lifetime of NH_3, and the limitation on transport of NH_3 to the site by the terrain (i.e. representativeness problems). Because no uniform criterion was found that would enable a good comparison for all stations, multiple criteria with a maximum difference of between 10 and 50 km will be used to analyze the optimal setting for each of the sites. Vertical sampling differences are not taken into consideration in this study. However, the IASI selection criterion on the thermal contrast is conservative, and only those measurements for which IASI has a good sensitivity to surface concentrations are selected.

Table 1. FTIR stations used in the analysis. The location, longitude, latitude, and altitude are given for each station as well as the instrument used for the measurements. Typical emission sources are mentioned in the station specifics tab. The topography describes the geography of the region surrounding the site. *N* gives the number of observations made during the period of interest. Time period gives the period from which data are used. The last column describes the used algorithm for the retrieval.

Station Location	Long	Lat	Altitude (m a.s.l.)	Instrument	Station specifics	Topography	Time period	*N*	Retrieval type
Bremen, Germany	8.85° E	53.10° N	27	Bruker 125 HR	City, fertilizers, livestock	Flat	2008–2015	278	Normal
Toronto, Canada	79.60° W	43.66° N	174	ABB Bomem DA8	City, fertilizers, biomass burning	On the edge of Lake Ontario	2008–2015	1167	Normal
Boulder, United States	105.26° W	39.99° N	1634	Bruker 120 HR	Fertilizers, biomass burning, livestock	Mountain range to the west	2010–2015	440	Normal
Tsukuba, Japan	140.13° E	36.05° N	31	Bruker 125 HR	Fertilizers, city	Mostly flat, hills to the north	2014–2015	66	Normal
Pasadena, United States	118.17° W	34.20° N	460	MKIV_JPL	City, fertilizers, biomass burning	Mountain range to the east	2010–2015	695	Normal
Mexico City, Mexico	99.18° W	19.33° N	2260	Bruker Vertex 80	City, fires, fertilizers	In between mountain ranges	2012–2015	3980	Normal
Saint-Denis, Réunion	55.5° E	20.90° S	85	Bruker 120 M	Fertilizers, biomass burning, remote	Volcanic	2008–2012	948	Wide
Wollongong, Australia	150.88° E	34.41° S	30	Bruker 125 HR	Fertilizers, biomass burning, low emissions	Coastal, hills to the west	2008–2015	3641	Wide
Lauder, New Zealand	169.68° E	45.04° S	370	Bruker 120 HR	Fertilizers, livestock	Hills	2008–2015	1784	Normal

Table 2. Applied data filters to the IASI-NH_3 product.

Filter	Filter criteria
Elevation	|FTIR station – IASI_Observation| < 300 m
Thermal contrast	Thermal contrast > 12 K
Surface temperature	$T > 275.15$ K
IASI-NH_3 retrieval error	None
Cloud cover fraction	< 10 %
Spatial sampling difference	50 km → 10 km, $\Delta x = 5$ km
Temporal sampling difference	< 90 min

Topography

Any hill or mountain range located between the satellite pixel and the FTIR station may inhibit transport and decrease their comparability. To account for the topography we only used observations that have at maximum an altitude difference of 300 m (in) between the location of the FTIR and the IASI pixel position. The 300 m criterion was chosen based on tests using the FTIR and satellite observations from Lauder. For the calculation of the height differences we used the Space Shuttle Radar Topography Mission Global product at 3 arcsec resolution (SRTMGL3, Farr et al., 2007).

Temporal variation

NH_3 concentrations can vary considerably during the day, with lifetimes as short as a few hours not being uncommon (Dentener and Crutzen, 1994; Bleeker et al., 2009). The variability of the concentrations mainly arises from the variability in emission strengths as influenced by agricultural practices; meteorological and atmospheric conditions such as temperature, precipitation, wind speed, and direction; the development of the boundary layer (which is important as the IASI satellite observations take place around 09:30 local time and thus the boundary layer has not always been fully established), pollution level, and deposition rates. To minimize the effects of this variability on the comparability of the IASI and FTIR observations, satellite observations with a time difference to FTIR observation of no more than 90 min were used.

Product error

The error of the IASI-NH_3 columns derives from errors on the HRI and the thermal contrast (Van Damme et al., 2014a). Applying relative error filters of 50, 75, and 100 % showed that mostly lower concentrations are removed from the comparison. Consequently, introducing any criteria based on the associated (relative) error will bias any comparison with FTIR columns towards the higher IASI total columns. Therefore, we decided not to filter based on the relative error as it skews the range of NH_3 column totals.

Meteorological factors

The lowest detectable total column of the retrieval depends on the thermal contrast of the atmosphere (Van Damme et al., 2014a). For example, the retrieval has a minimum detectable NH_3 column of around 5×10^{15} molecules cm^{-2} at a thermal contrast of about 12 K for columns using the "transported" profile. A thermal contrast of 12 K is chosen as the threshold to ensure the quality of the IASI observations, which represents a lapse rate of around 8 K km^{-1} altitude, near standard atmospheric conditions. We excluded data for T_{skin} temperatures below 275.15 K to introduce a basic filter for snow cover and conditions with frozen soils. The T_{skin} temperatures are obtained from the IASI L2 temperature profiles, which have an uncertainty of ~ 2 K at the surface (August et al., 2012). Finally, only IASI observations with a cloud cover below 10 % are used.

The complete list of selection criteria is summarized in Table 2.

Quality of the FTIR observations

No filters were applied to maximize the number of observations usable in the comparison. The resolution and detection limit of the FTIR instruments is usually better than that of the IASI instrument, leading to retrieved columns with, in principle, less uncertainty. Overall the FTIR retrievals show an error of ~ 30 % or less with the largest errors due to the spectroscopic parameters (Dammers et al., 2015). While artefacts are possible in the data we did not investigate for specific artefacts and possible impacts.

2.3.2 Application of averaging kernels

When performing a direct comparison between two remote sensing retrievals, one should take into account the vertical sensitivity and the influence of a priori profiles of both methods. One method to remove the influence of the a priori profile and the vertical sensitivity is the application of the averaging kernels of both retrievals to the retrieved profiles of both products. The IASI-NH_3 HRI-based product scheme, however, does not produce averaging kernels. Thus it is not possible to account for the vertical sensitivity of the satel-

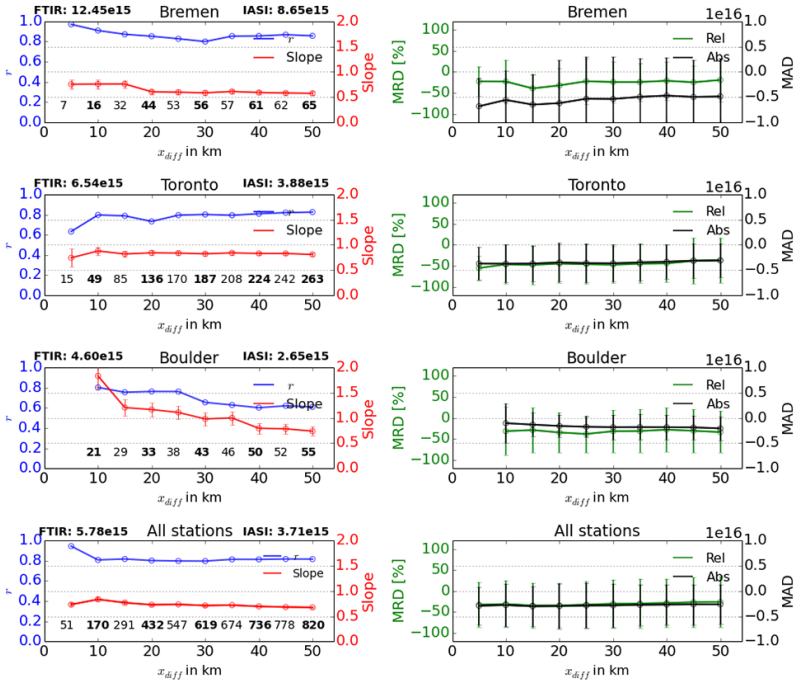

Figure 3. Correlation r (blue lines, left figures), slope (red lines, left figures) regression results, mean relative difference (MRD, green lines, right figures) and mean absolute difference (MAD, black lines, right figures) between IASI and FTIR observations as a function of x_{diff} for a selection of sites. Bars indicate the standard deviation of the slope of the individual regression results. The numbers in the bottom of each subfigure show the number of matching observations. The numbers on the left and right side of the stations name give the mean FTIR and IASI total columns for an $x_{\mathrm{diff}} < 25$ km.

lite retrieval. The effect of the lack of the satellite averaging kernel is hard to predict, so the satellite vertical sensitivity is only taken into account through the selection criterion on the thermal contrast. Nonetheless following the method described in Rodgers and Connor (2003), the FTIR averaging kernel $\mathbf{A}$ is applied to the IASI profile $\boldsymbol{x}_{\mathrm{sat}}$ to account for the effects of the a priori information and vertical sensitivity of the FTIR retrieval (the assumed profiles, called "land" and "sea" are described in Van Damme et al., 2014a). The IASI profiles are not fully retrieved profiles but fixed shape profiles used as an assumption in the IASI retrieval (see Van Damme et al., 2015a). These fixed profiles are used for scaling purposes to be able to account for the FTIR averaging kernel. A total column averaging kernel could be used instead, but in principle is similar to the procedure described here. The IASI profile is first mapped to the altitude grid of the FTIR profile by using interpolation, forming $\boldsymbol{x}_{\mathrm{sat}}^{\mathrm{mapped}}$. Applying Eq. (1), the smoothed IASI profile $\hat{x}_{\mathrm{sat}}$ is calculated indicating what the FTIR would retrieve when observing the satellite profile, which is then used to compute a total column. This profile can then be compared with the FTIR profile.

$$\hat{x}_{\mathrm{sat}} = \boldsymbol{x}_{\mathrm{ftir}}^{\mathrm{apriori}} + \mathbf{A}(\boldsymbol{x}_{\mathrm{sat}}^{\mathrm{mapped}} - \boldsymbol{x}_{\mathrm{ftir}}^{\mathrm{apriori}}) \quad (1)$$

After the application of the averaging kernel, for each FTIR observation, all satellite observations meeting the coincident criteria are averaged into a single mean total column value to be compared with the FTIR value. If multiple FTIR observations match a single satellite overpass, taking into account the maximum time difference, the FTIR observations are also averaged into a single mean total column value.

3 Results

3.1 The influence of spatial differences between observations

Following the approach of Irie et al. (2012) we will first show the correlation r, the slope as well as the mean relative difference (MRD), and the mean absolute difference (MAD) between satellite (y axis) and FTIR NH_3 total columns (x axis) for each of the sites, as a function of the maximum allowable spatial difference between the observations (x_{diff}). The relative difference (RD) is defined here as

$$\mathrm{RD} = \frac{(\text{IASI column} - \text{FTIR column}) \times 100}{\text{FTIR column}}. \quad (2)$$

A maximum relative difference of 200 % was used to remove extreme outliers from the data, typically observations under wintertime conditions. The left side of Fig. 3 shows the correlation coefficients (blue lines) and slope (red lines) for a

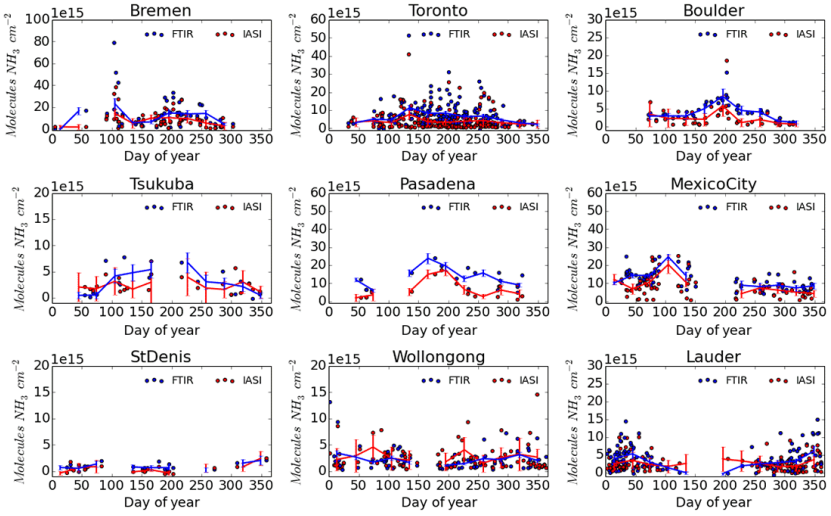

Figure 4. Time series of NH_3 for IASI and FTIR datasets with $x_{diff} < 25$ km and $t_{diff} < 90$ min (FTIR: blue and IASI: red). Scattered values are the observations for each day of year (multiple years of observations). The lines show the monthly mean total columns of the respective sets.

selection of sites as a function of x_{diff} using a maximum allowed sampling time difference of 90 min. The right side of Fig. 3 shows the MRD and MAD between the satellite and FTIR observations as a function of x_{diff}. The numbers on the bottom of each of the subfigures show the number of observations used in the comparison. The values in bold beside the title of each subplot give the mean concentrations of the IASI and FTIR observations. The bars indicate the standard deviation of the slope (left-side figures) and the relative and absolute differences (right-side figures).

For most stations an increasing x_{diff} (Fig. 3) means a decreasing correlation (blue lines) and a changing slope (either decreasing or increasing with distance, red lines). This can be explained by the local character and high variation of NH_3 emissions/concentration in combination with the locations of the stations. Moving further away from a source will then generally decrease the relation between the concentration in the air and the emission source. The same is true for satellite observations of the air concentrations, which have a large footprint compared to the local character of a point measurement (FTIR) and the emissions. The steepness of this decrease (or increase) tells us something about the local variation in NH_3 concentrations, which can be large for sites near heterogeneous emission sources or in cases with low transport/turbulence and thus overall relatively low mixing.

Overall the highest correlations are seen at the Bremen site, which can partially be explained by the overall high number of observations with high concentrations (more than $15–20 \times 10^{15}$ molecules cm^{-2}), which generally favours the correlations. The mean column totals as well as the MRD and MAD do not change much except for the smallest x_{diff} criteria. The larger changes for observations within 15 km are probably due to the smaller number of observations (which follows from the relatively few IASI observations directly above or near the stations). The results show an underestimation of observed columns by IASI with the "all stations" slopes in between $\sim 0.6–0.8$. The stations with a lower mean FTIR column totals, such as Toronto and Boulder (as well as Pasadena, Mexico City, and Lauder shown in Appendix Fig. A1), show lower correlations with most having slopes below 1. The correlations decreasing with mean column totals point towards the product detection limits of the IASI-NH_3 product. The Toronto site has lower correlation coefficients for the smallest xdiffs, but this seems to be due to the large drop in number of observations for an x_{diff} of < 15 km. For higher x_{diff} criteria the correlation of the Toronto site shows results similar to Bremen. The observations at Boulder also show large differences when including more observations further away from the station. This can be explained by the land use surrounding the Boulder site. Immediately west of the measurement site is a mountain range which together with our elevation filter leads to rejection of the observations to the west. To the northeast there are some major farming areas surrounding the river banks. Correlations do increase with a decreasing x_{diff}, suggesting that IASI is able to resolve the large gradients in the NH_3 concentrations near the site.

From the correlation analysis as a function of spatial coincidence, we conclude that an x_{diff} value of 25 km is recommended to make a fair comparison between IASI-NH_3 and FTIR. Any criterion smaller than 15 km greatly reduces the number of observations and statistics. x_{diff} values beyond 25 km further decrease the correlations for the combined set. From this point onward an x_{diff} value of 25 km will be used.

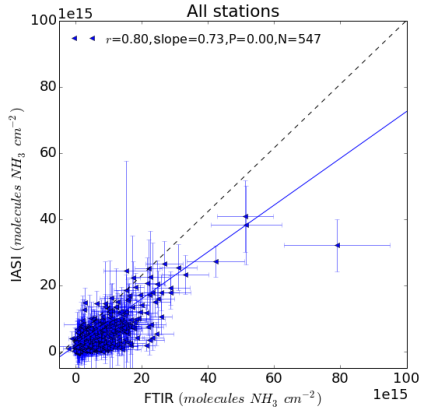

Figure 5. Correlations between the FTIR and IASI total columns with filters thermal contrast > 12 K, $t_{diff} < 90$ min, $x_{diff} < 25$ km. The trend line shows the results of the regression analysis.

Table 3. Summarized results of the comparison between FTIR-NH_3 and IASI-NH_3 total columns within the coincidence criteria threshold ($x_{diff} < 25$ km, $t_{diff} < 90$ min). N is the number of averaged total columns, MRD is the mean relative difference (in %), r and slope are the correlation coefficient and slope of the linear regression.

Sites	N	MRD in % (rms 1σ)	r	slope
Bremen	53	$-22.5 \pm (54.0)$	0.83	0.60
Toronto	170	$-46.0 \pm (47.0)$	0.79	0.84
Boulder	38	$-38.2 \pm (43.5)$	0.76	1.11
Tsukuba	15	$-28.3 \pm (35.6)$	0.67	0.57
Pasadena	16	$-47.9 \pm (30.1)$	0.59	0.83
Mexico	65	$-30.8 \pm (43.9)$	0.64	1.14
Saint Denis	20	$-61.3 \pm (78.7)$	0.65	1.26
Wollongong	62	$6.0 \pm (74.3)$	0.47	0.92
Lauder	108	$-29.7 \pm (57.3)$	0.55	0.77
Combined	547	$-32.4 \pm (56.3)$	0.80	0.73

3.2 Comparison of FTIR and IASI NH_3 data

Observations from multiple years are used to show the coincident seasonal variability of the FTIR and IASI-NH_3 products for each of the sites (Fig. 4, FTIR: blue, IASI: red). Observations are grouped together into a typical year as there are insufficient collocated observations to show an interannual time series. Note the different scales on the y axis. Similar seasonal cycles are clearly observed in both datasets for most stations. Enhanced concentrations in spring are observed for Bremen and Toronto as well as Boulder due to manure application. Most of the sites show an increase of NH_3 during the summer months, which is likely due to the increased volatilization of NH_3 as an effect of higher temperatures. Fire events that were captured earlier by FTIR at Saint Denis in November, as well as in the IASI data, are not observed in the collocated sets, which is due to a lack of coincident observations. Furthermore, there is a lack of observations in wintertime for most of the stations either due to low thermal contrast or due to overcast conditions. Tsukuba has observations above the detection limit but only 1 year of infrequent observations, which is insufficient to show an entirely clear seasonal cycle. A similar thing can be said for Pasadena, where there are too few coincident observations to make meaningful conclusions about the seasonal cycle. In conclusion, IASI reflects similar pollution levels and seasonal cycles as deduced from the FTIR observations.

Figures 5 and 6 show a direct comparison of the FTIR and IASI NH_3 total columns for each station as well as a combination of all the observations. Correlations, number of observations, and slope are shown in the figures. The MRD and these statistics are also summarized in Table 3. The comparison shows a variety of results. As before, of all nine stations Bremen shows the best correlation with a coefficient of determination of $r = 0.83$ and a slope of 0.60. The intercept is not fixed at zero. The stations with overall lower observed total columns (less than 10×10^{15} molecules cm^{-2}) show lower correlations. Stations with intermediate concentrations like Toronto and Boulder show correlations $r = \sim 0.7$–0.8. Figure 5 also shows the relatively low number of high observations for both the FTIR and IASI values as a result of the relatively few FTIR observations during events. The few outliers can have a disproportional effect on the slope as most of the lower observations are less accurate due to the detection limits of the instruments. Overall most stations, except Saint Denis, Boulder, and Mexico City, indicate an underestimation by IASI of the FTIR columns ranging from 10 to 50 %. The mean relative differences for most stations are negative with most showing values within $-22.5 \pm (54.0)$ % for Bremen down to a $-61.3 \pm (78.7)$ % for Saint Denis. The bias shows some dependence on the total columns with the underestimation being higher at stations with high mean total columns and lower at stations with low mean total columns. An exception to this is stations with the lowest mean total columns (i.e. Saint Denis and Wollongong). The differences at Saint Denis could be explained by the fact that most IASI observations are positioned above water due to restrictions for terrain height differences. A similar thing can be said for Wollongong, which is situated on the coast with hills directly to the inland. Most observations are on the border of water and land, which might introduce errors in the retrieval. The combination of all observations gives a MRD of $-32.4 \pm (56.3)$ %.

4 Discussion and conclusions

Recent satellite products enable the global monitoring of atmospheric concentrations of NH_3. Unfortunately, the validation of the satellite products of IASI (Van Damme et al., 2014a), TES (Shephard et al., 2011), and CrIS (Shephard and Cady-Pereira, 2015) is very limited and, so far, only based

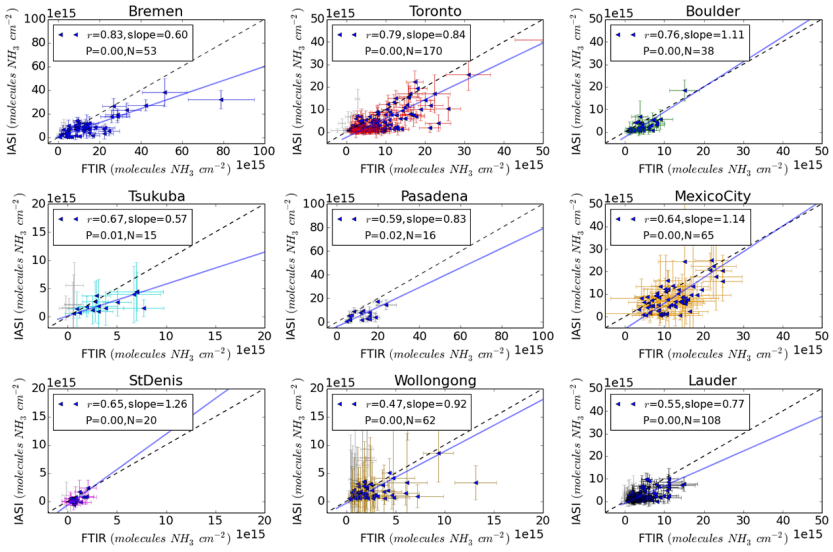

Figure 6. Correlations between the FTIR and IASI total columns with filters thermal contrast > 12, $t_{\mathrm{diff}} < 90$ min, $x_{\mathrm{diff}} < 25$ km. The trend lines show the results of the regression analysis.

on sparse in situ and airborne studies. Dammers et al. (2015) presented FTIR total column measurements of NH_3 at several places around the world and demonstrated that these data can provide information about the temporal variation of the column concentrations, which are more suitable for validation than ground-level concentrations. Ground-based remote sensing instruments have a long history for validation of satellite products. FTIR observations are already commonly used for the validation of many satellite products, including carbon monoxide (CO), methane (CH_4), and nitrous oxide (N_2O) (Wood, 2002; Griesfeller et al., 2006; Dils et al., 2006; Kerzenmacher et al., 2012). Furthermore, MAX-DOAS systems are used for the validation of retrievals for reactive gases (e.g. Irie et al., 2012), whereas AERONET is widely used to validate satellite-derived aerosol optical depth (e.g. Schaap et al., 2008). The comparison between FTIR and IASI NH_3 column reported here can be seen as a first step in the validation of NH_3 satellite products.

In this study, we collected FTIR measurements from nine locations around the world and followed the retrieval described by Dammers et al. (2015). The resulting datasets were used to quantify the bias and evaluate the seasonal variability in the IASI-NH_3 product. Furthermore, we assessed the colocation criteria for the satellite evaluation. Additional selection criteria based on thermal contrast, surface temperature, cloud cover, and elevation differences between observations were applied to ensure the quality of the IASI-NH_3 observations. The FTIR averaging kernels were applied to the satellite profiles to account for the vertical sensitivity of the FTIR and the influence of the a priori profiles.

To optimally compare the satellite product to the FTIR observations it is best to reduce the spatial collocation criterion to the size of the satellite instrument's footprint and allow for a time difference as short as possible. These considerations are to reduce effects of transport, chemistry, and boundary layer growth but limit the number of coinciding observations significantly. We have shown that the spatial distance between the IASI observations and the FTIR measurement site is of importance: the larger the distance in space, the lower the correlation. When there is no exact match in the position of both observations the variations in the spatial separation lead to correlation coefficients that can greatly change even when changing the spatial criteria (x_{diff}) from 10 to 30 km. Reasons for the changes are the local nature of NH_3 emissions, the surrounding terrain characteristics, and their influence on local transport of NH_3. The small values for spatial and temporal coincidence criteria show the importance of NH_3 sources near the measurement sites when using these observations for satellite validation. For the validation of the IASI observations, we used an x_{diff} of less than 25 km, which still showed high correlations while a large number of observations are retained for comparison.

Overall we see a broad consistency between the IASI and FTIR observations. The seasonal variations of both datasets look similar for most stations. Increased column values are observed for both IASI and FTIR during summers as the result of higher temperatures, with some sites showing an increase in concentrations due to manure application and fertilization events in spring (Bremen, Toronto). In general our comparison shows that IASI underestimates the NH_3 total columns, except for Wollongong. The Wollongong site has persistent low background columns, i.e. observations with a low HRI, to which IASI is not very sensitive, which results in an overestimation of the observed columns. Overall, correlations range from $r \sim 0.8$ for stations characterized by higher NH_3 column totals (with FTIR columns up to

80×10^{15} molecules cm^{-2}) to low $r \sim 0.4$–0.5 correlations for stations, which only have a few to no FTIR observations above 5×10^{15} molecules cm^{-2}. Hence, the detection limit or sensitivity of the IASI instrument largely explains the lower correlation values. The combination of all sites ($N_{obs} = 547$) gives a MRD of $-32.4 \pm (56.3)\,\%$, a correlation r of 0.8 with a slope of 0.73.

In comparison to ground-based in situ systems, the FTIR observations have the big advantage to provide coarse vertical profiles, from which a column can be derived, which are more similar to what the satellite measures and therefore more useful for validation. Dedicated NH_3 validation datasets are needed that better match the overpass times of satellite instruments like IASI, TES, and CrIS. This could be achieved by the addition of NH_3 to the NDACC measurement protocols and matching the overpass time of these satellites over these measurement stations by using of the right spectral filters for detecting NH_3. Furthermore, the low number of NDACC stations and their locations are not optimal for a dedicated validation of NH_3 satellite products. Although these provide a starting point, the small set of stations does not cover the entire range of climate conditions, agricultural source types, and emission regimes. Hence, our validation results should be seen as indicative. Additional stations or dedicated field campaigns are needed to improve this situation. New stations should be placed in regions where emissions and geography are homogenous to ensure that stations are representative for the footprints of the satellites. For validation of satellite products using FTIR measurements a monitoring and measurements strategy needs to be developed with a representative mixture of locations in addition to ground-level data. The latter can cover the spatial variation, and different temporal measurements can be used. The use of IASI and FTIR observations to study NH_3 distributions at ground level requires a combination of model calculations and observations (e.g. Erisman et al., 2005a, b). Such techniques are required to provide all the necessary details to describe the high spatial and temporal variations in NH_3.

The direct comparison of the IASI and FTIR columns is an addition to earlier efforts by Van Damme et al. (2015a) to validate IASI column observations with surface in situ and airborne observations. Our results presented here indicate that the product performs better than the previous upper-bound estimate of a factor of 2 (i.e. -50 to $+100\,\%$) as reported in Van Damme et al. (2014a). Although we tried to diminish any effect of sampling time and position, it cannot be ruled out completely that these impact the comparison statistics as the number of stations is small. Still the picture arising from the different stations is rather consistent, which hints at other issues that may explain the observed bias. A number of important issues concerning the retrieval techniques may explain the observed difference. First, the HRI-based retrieval used for IASI is intrinsically different to the optimal estimation-based approach used for the FTIR retrieval. An IASI optimal estimation retrieval for NH_3 called FORLI does exist but is not fully operationally used as it is computationally much slower than the HRI method. Surprisingly a first comparison between the FORLI- and HRI-based retrieval (see Fig. 9, Van Damme et al., 2014a) shows $\sim 30\,\%$ lower retrieved columns by the HRI scheme, which is very close to the systematic difference quantified here. Note that the results are not fully comparable as the reported HRI–FORLI comparison was for a limited dataset and no quality selection criteria were applied. We recommend to further explore the use of the optimal estimation-based IASI-NH_3 retrieval in comparison to the FTIR observations. Second, the IASI and FTIR retrievals incorporate the same line spectroscopy database (HITRAN 2012; Rothman et al., 2013), which removes a possible error due to different spectroscopy datasets. The spectroscopy is the largest expected cause of error in the FTIR observations with measurement noise being the close second for sites with low concentrations. An improvement to the line parameters (i.e. line intensity, pressure, and temperature effects) would greatly benefit both the FTIR and IASI retrievals. Thirdly, the HRI-based scheme uses the difference between spectra with and without the spectral signature of NH_3. A plausible cause for error in this scheme is the influence and correlation of interfering species in the same spectral channels. H_2O lines occur near most of the NH_3 spectral lines and interfere with the NH_3 lines at the resolution of the IASI instrument. Humidity levels vary throughout the year with an increased amount of water vapour in summer conditions. The HRI-based scheme uses a fixed amount of water vapour, and varying amounts of water vapour may interfere with the HRI value attributed fully to the NH_3 columns. As there is a seasonality in the water vapour content of the atmosphere (Wagner et al., 2006), any error attributed to water vapour should show a seasonality in the difference between the IASI and FTIR observations. A seasonality was, however, not visible although it may be that the number of coincident observations was too small to recognize it. This again shows the need for dedicated NH_3 validation data (e.g. dedicated FTIR observations). Fourth, the negative bias of the satellite observations can be expected by the lack of sensitivity to concentrations near the surface. This is of course where the ammonia concentrations usually peak. The FTIR observations however do fully observe the lower layers in the troposphere, thus causing a discrepancy. Normally one can correct for this using the averaging kernel of the satellite observations. However, the IASI-NH_3 retrieval does not produce an averaging kernel, meaning it is not possible to calculate the exact effect. The use of a typical averaging kernel will cause more uncertainty as there is a large day-to-day variability in the averaging kernels as earlier retrievals showed (Clarisse et al., 2009). Finally, another possible cause of error is the lack of a varying NH_3 profile and the proxy used for thermal contrast to describe the state of the atmosphere. The sensitivity of the scheme to the concentrations of NH_3 in the boundary layer is described by using a fixed profile for land and sea observations in combination with a thermal contrast based on two layers (surface and

1.5 km) as it is expected that most of the NH_3 occurs in the boundary layer. In reality the NH_3 profile is highly dynamic due to a varying boundary layer height and changing emissions as well as temperature changes (e.g. inversions) occurring throughout the planetary boundary layer. Not accounting for this can introduce an error and future HRI-based schemes should focus on estimating the possible effects of using only a specific profile. The use of multiple NH_3 profiles in combination with multiple temperature layers would be a better approximation of the state of the atmosphere, although computationally more expensive. The sharp difference between the sea and land retrieval introduces strong variability in observations near the coast. Furthermore, observations that are directly on the transition between water and land can introduce problems due to the varying emissivity. Similar issues have been reported for aerosol retrievals (e.g. Schaap et al., 2008).

Although the FTIR observations offer some vertical information, studies combining this technique with tower or airborne observations are needed to further improve knowledge and sensitivity of the FTIR and satellite observations to the vertical distribution of NH_3. Without this knowledge, it is not possible to use the observations for quantitative emission estimates and modelling purposes as no uncertainty on the new estimate can be given. Approaches similar to the recent study by Shephard et al. (2015) using an airborne instrument, possibly in combination with an FTIR system focused on the overpass of multiple satellite systems for an extended period of time, should be used to establish the sensitivities and biases of the different retrieval products available from satellite instruments as well as the bias between the satellite and surface instruments. The use of IASI and FTIR observations to study NH_3 distributions at ground level requires a combination of model calculations and observations. Such techniques are required to provide all the necessary details to describe the high spatial and temporal variations in NH_3.

5 Data availability

The IASI-NH3 product is freely available at http://www.pole-ether.fr/etherTypo/index.php?id=1700&L=1 (Van Damme et al., 2015a). FTIR-NH3 data (Dammers et al., 2015) can be made available on request (M. Palm, Institut für Umweltphysik, University of Bremen, Bremen, Germany).

Appendix A

This section further covers the other stations, in addition to the sites covered by Sect. 3.1.

The results for Mexico City show an overall constant correlation coefficient except for small criteria < 20 km. The slope also decreases towards values seen at other stations. This effect could be due to a large number of sources inside the city, i.e. automobile and agricultural emissions in and near the city, increasing the heterogeneity of the found column totals. Réunion and Tsukuba have few coincident observations leading to only a few significant comparisons. This, combined with the low concentrations measured at Réunion, leads to large differences in the mean and standard deviations of the subsequent x_{diff} sets. The Réunion and Wollongong observations are at the sensitivity limit of the IASI-NH_3 retrieval, which limits the usefulness of the sites for the validation. As there are only a few observations for Tsukuba it is hard to make meaningful conclusions on the variability around the site.

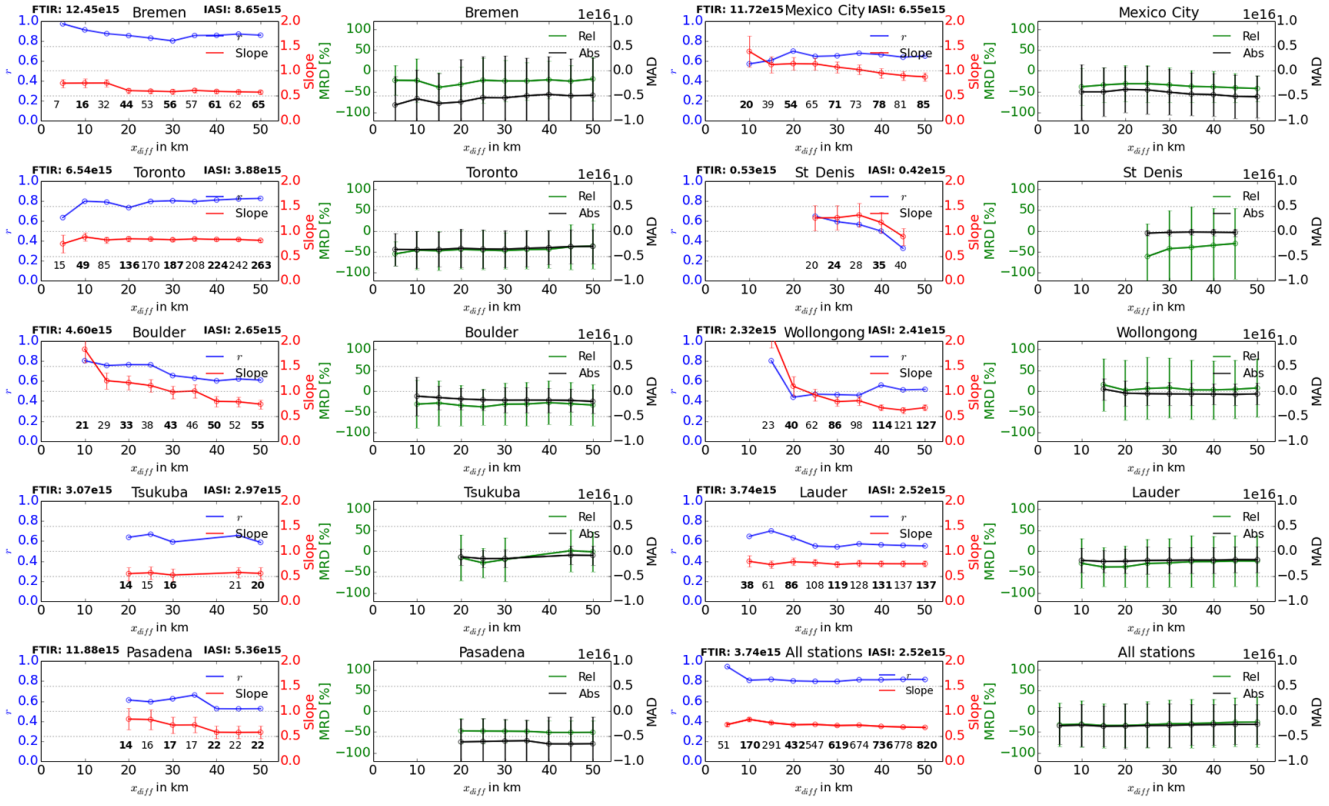

Figure A1. Correlation r (blue lines, left figures), slope (red lines, left figures) regression results, mean relative difference (MRD, green lines, right figures) and mean absolute difference (MAD, black lines, right figures) between IASI and FTIR observations as a function of x_{diff} for all sites. Bars indicate the standard deviation of the slope of the individual regression results. The numbers in the bottom of each subfigure show the number of matching observations. The numbers on the left and right side of the station name give the mean FTIR and IASI total columns for an $x_{\mathrm{diff}} < 25$ km.

Acknowledgements. This work is part of the research programme GO/12-36, which is financed by the Netherlands Organisation for Scientific Research (NWO). The Lauder NIWA FTIR programme is funded through the New Zealand government's core research grant framework from the Ministry of Business, Innovation and Employment. We thank the Lauder FTIR team for their contribution. We acknowledge the Université de La Réunion and CNRS (LACy-UMR8105 and UMS3365) for their support of the Réunion Island measurements. The Réunion Island data analysis has mainly been supported by the A3C project (PRODEX Programme of the Belgian Science Policy Office, BELSPO, Brussels). The University of Toronto's NDACC contribution has been supported by the CAFTON project, funded by the Canadian Space Agency's FAST programme. Measurements were made at the University of Toronto Atmospheric Observatory (TAO), which has been supported by CFCAS, ABB Bomem, CFI, CSA, EC, NSERC, ORDCF, PREA, and the University of Toronto. Part of this research was performed at the Jet Propulsion Laboratory, California Institute of Technology, under contract with NASA. IASI has been developed and built under the responsibility of the "Centre national d'études spatiales" (CNES, France). It is flown on-board the Metop satellites as part of the EUMETSAT Polar System. The IASI L1 data were received through the EUMETCast near-real-time data distribution service.

The IASI-related activities in Belgium were funded by Belgian Science Policy Office through the IASI Flow Prodex arrangement (2014–2018). Pierre.-F. Coheur, Lieven Clarisse, and Martin Van Damme also thank the FRS-FNRS for financial support. Lieven Clarisse is a research associate with the Belgian F.R.S-FNRS. Cathy Clerbaux is grateful to CNES for scientific collaboration and financial support. The National Center for Atmospheric Research is supported by the National Science Foundation. The Boulder observation programme is supported in part by the Atmospheric Chemistry Observations & Modeling Division of NCAR. The measurement programme and NDACC site at Wollongong have been supported by the Australian Research Council for many years, most recently by grants DP110101948 and LE0668470. The Mexico City site was funded through projects UNAM-DGAPA (109914) and CONACYT (249374, 239618). A. Bezanilla, J. Baylón, and E. Plaza are acknowledged for their participation in the measurements and analysis. We would like to thank David Griffith, Clare Murphy, and Voltaire Velazco at the School of Chemistry, University of Wollongong, for maintaining Fourier transform spectroscopy (FTS) instrumentation and conducting FTS measurements. We are grateful to the many colleagues who have contributed to FTIR data acquisition at the various sites.

Edited by: R. Müller
Reviewed by: two anonymous referees

References

Adams, P. J., Seinfeld, J. H., Koch, D., Mickley, L., and Jacob, D.: General circulation model assessment of direct radiative forcing by the sulfate-nitrate-ammonium-water inorganic aerosol system, J. Geophys. Res.-Atmos., 106, 1097–1111, 2001.

August, T., Klaes, D., Schlüssel, P., Hultberg, T., Crapeau, M., Arriaga, A., O'Carroll, A., Coppens, D., Munro, R., and Calbet, X.: IASI on Metop-A: Operational Level 2 retrievals after five years in orbit, J. Quant. Spectrosc. Ra., 113, 1340–1371, doi:10.1016/j.jqsrt.2012.02.028, 2012.

Beer, R., Shephard, M. W., Kulawik, S. S., Clough, S. a., Eldering, A., Bowman, K. W., Sander, S. P., Fisher, B. M., Payne, V. H., Luo, M., Osterman, G. B., and Worden, J. R.: First satellite observations of lower tropospheric ammonia and methanol, Geophys. Res. Lett., 35, 1–5, doi:10.1029/2008GL033642, 2008.

Bleeker, A., Sutton, M. A., Acherman, B., Alebic-Juretic, A., Aneja, V. P., Ellermann, T., Erisman, J. W., Fowler, D., Fagerli, H., Gauger, T., Harlen, K. S., Hole, L. R., Horvath, L., Mitosinkova, M., Smith, R. I., Tang, Y. S., and Pul, A.: Linking ammonia emission trends to measured concentrations and deposition of reduced nitrogen at different scales, in: Atmospheric Ammonia – Detecting emission changes and environmental impacts. Results of an expert workshop under the convention of long-range transboundary air pollution, edited by: Sutton, M. A., Reis, S., and Baker, S. M. H., Atmospheric Ammonia – Detecting emission changes and environmental impacts, Springer, 123–180, 2009.

Bobbink, R., Hicks, K., Galloway, J., Spranger, T., Alkemade, R., Ashmore, M., Bustamante, M., Cinderby, S., Davidson, E., Dentener, F., Emmett, B., Erisman, J. W., Fenn, M., Gilliam, F., Nordin, A., Pardo, L., and De Vries, W.: Global assessment of nitrogen deposition effects on terrestrial plant diversity: a synthesis, Ecol. Appl., 20, 30–59, 2010.

Brown, L. R., Gunson, M. R., Toth, R. A., Irion, F. W., Rinsland, C. P., and Goldman, A.: 1995 atmospheric trace molecule spectroscopy (ATMOS) linelist, Appl. Optics, 35, 2828–2848, 1996.

Chang, L., Palo, S., Hagan, M., Richter, J., Garcia, R., Riggin, D., and Fritts, D.: Structure of the migrating diurnal tide in the Whole Atmosphere Community Climate Model (WACCM), Adv. Space Res., 41, 1398–1407, doi:10.1016/j.asr.2007.03.035, 2008.

Clarisse, L., Clerbaux, C., Dentener, F., Hurtmans, D., and Coheur, P.-F.: Global ammonia distribution derived from infrared satellite observations, Nat. Geosci., 2, 479–483, 2009.

Clarisse, L., Shephard, M. W., Dentener, F., Hurtmans, D., Cady-Pereira, K., Karagulian, F., Van Damme, M., Clerbaux, C., and Coheur, P.-F.: Satellite monitoring of ammonia: A case study of the San Joaquin Valley, J. Geophys. Res., 115, 1–15, doi:10.1029/2009JD013291, 2010.

Coheur, P.-F., Clarisse, L., Turquety, S., Hurtmans, D., and Clerbaux, C.: IASI measurements of reactive trace species in biomass burning plumes, Atmos. Chem. Phys., 9, 5655–5667, doi:10.5194/acp-9-5655-2009, 2009.

Dammers, E., Vigouroux, C., Palm, M., Mahieu, E., Warneke, T., Smale, D., Langerock, B., Franco, B., Van Damme, M., Schaap, M., Notholt, J., and Erisman, J. W.: Retrieval of ammonia from ground-based FTIR solar spectra, Atmos. Chem. Phys., 15, 12789–12803, doi:10.5194/acp-15-12789-2015, 2015.

Dentener, F. J. and Crutzen, P. J.: A three-dimensional model of the global ammonia cycle, J. Atmos. Chem., 19, 331–369, doi:10.1007/BF00694492, 1994.

Dentener, F., Drevet, J., Lamarque, J. F., Bey, I., Eickhout, B., Fiore, A. M., Hauglustaine, D., Horowitz, L. W., Krol, M., Kulshrestha, U. C., Lawrence, M., Galy-Lacaux, C., Rast, S., Shindell, D., Stevenson, D., Van Noije, T., Atherton, C., Bell, N., Bergman, D., Butler, T., Cofala, J., Collins, B., Doherty, R., Ellingsen, K., Galloway, J., Gauss, M., Montanaro, V., Müller, J. F., Pitari, G., Rodriguez, J., Sanderson, M., Solmon, F., Strahan, S., Schultz, M., Sudo, K., Szopa, S., and Wild, O.: Ni-

trogen and sulfur deposition on regional and global scales: A multimodel evaluation, Global Biogeochem. Cy., 20, GB4003, doi:10.1029/2005GB002672, 2006.

Dils, B., De Mazière, M., Müller, J. F., Blumenstock, T., Buchwitz, M., de Beek, R., Demoulin, P., Duchatelet, P., Fast, H., Frankenberg, C., Gloudemans, A., Griffith, D., Jones, N., Kerzenmacher, T., Kramer, I., Mahieu, E., Mellqvist, J., Mittermeier, R. L., Notholt, J., Rinsland, C. P., Schrijver, H., Smale, D., Strandberg, A., Straume, A. G., Stremme, W., Strong, K., Sussmann, R., Taylor, J., van den Broek, M., Velazco, V., Wagner, T., Warneke, T., Wiacek, A., and Wood, S.: Comparisons between SCIAMACHY and ground-based FTIR data for total columns of CO, CH_4, CO_2 and N_2O, Atmos. Chem. Phys., 6, 1953–1976, doi:10.5194/acp-6-1953-2006, 2006.

EDGAR-Emission Database for Global Atmospheric Research: Source: EC-JRC/PBL, EDGAR version 4.2., available at: http://edgar.jrc.ec.europa.eu (last access: 15 October 2012), 2011.

Erisman, J. W., Hensen, A., Mosquera, J., Sutton, M., and Fowler, D.: Deposition monitoring networks: what monitoring is required to give reasonable estimates of ammonia/ammonium?, Environ. Pollut., 135, 419–431, doi:10.1016/j.envpol.2004.11.015, 2005a.

Erisman, J. W., Vermeulen, A., Hensen, A., Flechard, C., Dämmgen, U., Fowler, D., Sutton, M., Grünhage, L., and Tuovinen, J. P.: Monitoring and modelling of biosphere/atmosphere exchange of gases and aerosols in Europe, Environ. Pollut., 133, 403–413, doi:10.1016/j.envpol.2004.07.004, 2005b.

Erisman, J. W., Bleeker, A., Galloway, J., and Sutton, M. S.: Reduced nitrogen in ecology and the environment, Environ. Pollut., 150, 140–149, doi:10.1016/j.envpol.2007.06.033, 2007.

Erisman, J. W., Sutton, M. A., Galloway, J., Klimont, Z., and Winiwarter, W.: How a century of ammonia synthesis changed the world, Nat. Geosci., 1, 636–639, doi:10.1038/ngeo325, 2008.

Erisman, J. W., Galloway, J., Seitzinger, S., Bleeker, A., and Butterbach-Bahl, K.: Reactive nitrogen in the environment and its effect on climate change, Curr. Opin. Environ. Sustain., 3, 281–290, doi:10.1016/j.cosust.2011.08.012, 2011.

Farr, T. G., Rosen, P. A., Caro, E., and Crippen, R.: The Shuttle Radar Topography Mission, Rev. Geophys., 45, RG2004, doi:10.1029/2005RG000183, 2007.

Fowler, D., Coyle, M., Skiba, U., Sutton, M. A., Cape, J. N., Reis, S., Sheppard, L. J., Jenkins, A., Grizzetti, B., Galloway, J. N., Vitousek, P., Leach, A., Bouwman, A. F., Butterbach-Bahl, K., Dentener, F., Stevenson, D., Amann, M., and Voss, M.: The global nitrogen cycle in the twenty-first century, Philos. T. R. Soc. Lond. B, 368, 1621, doi:10.1098/rstb.2013.0164, 2013.

Griesfeller, A., Griesfeller, J., Hase, F., Kramer, I., Loës, P., Mikuteit, S., Raffalski, U., Blumenstock, T., and Nakajima, H.: Comparison of ILAS-II and ground-based FTIR measurements of O_3, HNO_3, N_2O, and CH_4 over Kiruna, Sweden, J. Geophys. Res., 111, D11S07, doi:10.1029/2005JD006451, 2006.

Hase, F., Blumenstock, T., and Paton-Walsh, C.: Analysis of the instrumental line shape of high-resolution fourier transform IR spectrometers with gas cell measurements and new retrieval software., Appl. Optics, 38, 3417–3422, 1999.

Hase, F., Hannigan, J. W., Coffey, M. T., Goldman, a., Höpfner, M., Jones, N. B., Rinsland, C. P., and Wood, S. W.: Intercomparison of retrieval codes used for the analysis of high-resolution, ground-based FTIR measurements, J. Quant. Spectrosc. Ra., 87, 25–52, doi:10.1016/j.jqsrt.2003.12.008, 2004.

Hase, F., Demoulin, P., Sauval, A. J., Toon, G. C., Bernath, P. F., Goldman, A., Hannigan, J. W., and Rinsland, C. P.: An empirical line-by-line model for the infrared solar transmittance spectrum from 700 to 5000 cm^{-1}, J. Quant. Spectrosc. Ra., 102, 450–463, doi:10.1016/j.jqsrt.2006.02.026, 2006.

Holland, E. A., Dentener, F. J., Braswell, B. H., and Sulzman, J. M.: Contemporary and pre-industrial global reactive nitrogen budgets, Biogeochemistry, 46, 7–43, doi:10.1007/BF01007572, 1999.

Irie, H., Boersma, K. F., Kanaya, Y., Takashima, H., Pan, X., and Wang, Z. F.: Quantitative bias estimates for tropospheric NO_2 columns retrieved from SCIAMACHY, OMI, and GOME-2 using a common standard for East Asia, Atmos. Meas. Tech., 5, 2403–2411, doi:10.5194/amt-5-2403-2012, 2012.

Kerzenmacher, T., Dils, B., Kumps, N., Blumenstock, T., Clerbaux, C., Coheur, P.-F., Demoulin, P., García, O., George, M., Griffith, D. W. T., Hase, F., Hadji-Lazaro, J., Hurtmans, D., Jones, N., Mahieu, E., Notholt, J., Paton-Walsh, C., Raffalski, U., Ridder, T., Schneider, M., Servais, C., and De Mazière, M.: Validation of IASI FORLI carbon monoxide retrievals using FTIR data from NDACC, Atmos. Meas. Tech., 5, 2751–2761, doi:10.5194/amt-5-2751-2012, 2012.

Kuenen, J. J. P., Visschedijk, A. J. H., Jozwicka, M., and Denier van der Gon, H. A. C.: TNO-MACC_II emission inventory; a multi-year (2003–2009) consistent high-resolution European emission inventory for air quality modelling, Atmos. Chem. Phys., 14, 10963–10976, doi:10.5194/acp-14-10963-2014, 2014.

Leen, J. B., Yu, X. Y., Gupta, M., Baer, D. S., Hubbe, J. M., Kluzek, C. D., Tomlinson, J. M., and Hubbell, M. R.: Fast in situ airborne measurement of ammonia using a mid-infrared off-axis ICOS spectrometer, Environ. Sci. Technol., 47, 10446–10453, doi:10.1021/es401134u, 2013.

Luo, M., Shephard, M. W., Cady-Pereira, K. E., Henze, D. K., Zhu, L., Bash, J. O., Pinder, R. W., Capps, S. L., Walker, J. T., and Jones, M. R.: Satellite observations of tropospheric ammonia and carbon monoxide: Global distributions, regional correlations and comparisons to model simulations, Atmos. Environ., 106, 262–277, doi:10.1016/j.atmosenv.2015.02.007, 2015.

Lutsch, E., Dammers, E., Conway, S., and Strong, K.: Ground-based FTIR measurements of CO, HCN, C_2H_6 and NH_3 emissions from the 2014 Canadian Wildfires, Geophys. Res. Lett., 43, doi:10.1002/2016GL070114, 2016.

Morgenstern, O., Zeng, G., Wood, S. W., Robinson, J., Smale, D., Paton-Walsh, C., Jones, N. B., and Griffith, D. W. T.: Long-range correlations in Fourier transform infrared, satellite, and modeled CO in the Southern Hemisphere, J. Geophys. Res., 117, D11301, doi:10.1029/2012JD017639, 2012.

Moya, M., Fountoukis, C., Nenes, A., Matías, E., and Grutter, M.: Predicting diurnal variability of fine inorganic aerosols and their gas-phase precursors near downtown Mexico City, Atmos. Chem. Phys. Discuss., 7, 11257–11294, doi:10.5194/acpd-7-11257-2007, 2007.

Nowak, J. B., Neuman, J. A., Kozai, K., Huey, L. G., Tanner, D. J., Holloway, J. S., Ryerson, T. B., Frost, G. J., McKeen, S. A., and Fehsenfeld, F. C.: A chemical ionization mass spectrometry technique for airborne measurements of ammonia, J. Geophys. Res.-Atmos., 112, D10S02, doi:10.1029/2006JD007589, 2007.

Nowak, J. B., Neuman, J. A., Bahreini, R., Brock, C. A., Middlebrook, A. M., Wollny, A. G., Holloway, J. S., Peischl, J., Ryerson,

T. B., and Fehsenfeld, F. C.: Airborne observations of ammonia and ammonium nitrate formation over Houston, Texas, J. Geophys. Res.-Atmos., 115, D22304, doi:10.1029/2010JD014195, 2010.

Ohyama, H., Morino, I., Nagahama, T., Machida, T., Suto, H., Oguma, H., Sawa, Y., Matsueda, H., Sugimoto, N., Nakane, H., and Nakagawa, K.: Column-averaged volume mixing ratio of CO_2 measured with ground-based Fourier transform spectrometer at Tsukuba, J. Geophys. Res., 114, D18303, doi:10.1029/2008JD011465, 2009.

Paton-Walsh, C., Jones, N. B., Wilson, S. R., Haverd, V., Meier, A., Griffith, D. W. T., and Rinsland, C. P.: Measurements of trace gas emissions from Australian forest fires and correlations with coincident measurements of aerosol optical depth, J. Geophys. Res., 110, D24305, doi:24310.21029/22005JD006202, 2005.

Pope, III, C. A., Ezzati, M., and Dockery, D. W.: Fine-Particulate Air Pollution and Life Expectancy in the United States, N. Engl. J. Med., 360, 376–386, doi:10.1056/NEJMsa0805646, 2009.

Pougatchev, N. S., Connor, B. J., and Rinsland, C. P.: Infrared measurements of the ozone vertical distribution above Kitt Peak, J. Geophys. Res.-Atmos., 100, 16689–16697, 1995.

Puchalski, M. A., Sather, M. E., Walker, J. T., Lehmann, C. M., Gay, D. A., Mathew, J., and Robarge, W. P.: Passive ammonia monitoring in the United States: Comparing three different sampling devices, J. Environ. Monitor., 13, 3156–3167, doi:10.1039/c1em10553a, 2011.

Ravishankara, A. R., Daniel, J. S., and Portmann, R. W.: Nitrous oxide (N_2O): the dominant ozone-depleting substance emitted in the 21st century, Science, 326, 123–125, doi:10.1126/science.1176985, 2009.

Rockström, J., Steffen, W., Noone, K., Persson, A., Chapin, F. S., Lambin, E. F., Lenton, T. M., Scheffer, M., Folke, C., Schellnhuber, H. J., Nykvist, B., de Wit, C. A., Hughes, T., van der Leeuw, S., Rodhe, H., Sorlin, S., Snyder, P. K., Costanza, R., Svedin, U., Falkenmark, M., Karlberg, L., Corell, R. W., Fabry, V. J., Hansen, J., Walker, B., Liverman, D., Richardson, K., Crutzen, P., and Foley, J. A.: A safe operating space for humanity, Nature, 461, 472–475, doi:10.1038/461472a, 2009.

Rodgers, C. D.: Inverse Methods for Atmospheric Sounding – Theory and Practice, Series on Atmospheric, Oceanic and Planetary Physics: Volume 2, 256 pp., doi:10.1142/9789812813718, 2000.

Rodgers, C. D. and Connor, B. J.: Intercomparison of remote sounding instruments, J. Geophys. Res.-Atmos., 108, 4116, doi:10.1029/2002JD002299, 2003.

Rodhe, H., Dentener, F., and Schulz, M.: The global distribution of acidifying wet deposition, Environ. Sci. Technol., 36, 4382–4388, 2002.

Rothman, L. S., Gordon, I. E., Babikov, Y., Barbe, A., Chris Benner, D., Bernath, P. F., Birk, M., Bizzocchi, L., Boudon, V., Brown, L. R., Campargue, A., Chance, K., Cohen, E. A., Coudert, L. H., Devi, V. M., Drouin, B. J., Fayt, A., Flaud, J. M., Gamache, R. R., Harrison, J. J., Hartmann, J. M., Hill, C., Hodges, J. T., Jacquemart, D., Jolly, A., Lamouroux, J., Le Roy, R. J., Li, G., Long, D. A., Lyulin, O. M., Mackie, C. J., Massie, S. T., Mikhailenko, S., Müller, H. S. P., Naumenko, O. V., Nikitin, A. V., Orphal, J., Perevalov, V., Perrin, a., Polovtseva, E. R., Richard, C., Smith, M. A. H., Starikova, E., Sung, K., Tashkun, S., Tennyson, J., Toon, G. C., Tyuterev, V. G., and Wagner, G.: The HITRAN2012 molecular spectroscopic database, J. Quant. Spectrosc. Ra., 130, 4–50, doi:10.1016/j.jqsrt.2013.07.002, 2013.

Schaap, M., van Loon, M., ten Brink, H. M., Dentener, F. J., and Builtjes, P. J. H.: Secondary inorganic aerosol simulations for Europe with special attention to nitrate, Atmos. Chem. Phys., 4, 857–874, doi:10.5194/acp-4-857-2004, 2004.

Schaap, M., Timmermans, R. M. A., Koelemeijer, R. B. A., de Leeuw, G., and Builtjes, P. J. H.: Evaluation of MODIS aerosol optical thickness over Europe using sun photometer observations, Atmos. Environ., 42, 2187–2197, doi:10.1016/j.atmosenv.2007.11.044, 2008.

Senten, C., De Mazière, M., Dils, B., Hermans, C., Kruglanski, M., Neefs, E., Scolas, F., Vandaele, A. C., Vanhaelewyn, G., Vigouroux, C., Carleer, M., Coheur, P. F., Fally, S., Barret, B., Baray, J. L., Delmas, R., Leveau, J., Metzger, J. M., Mahieu, E., Boone, C., Walker, K. A., Bernath, P. F., and Strong, K.: Technical Note: New ground-based FTIR measurements at Ile de La Réunion: observations, error analysis, and comparisons with independent data, Atmos. Chem. Phys., 8, 3483–3508, doi:10.5194/acp-8-3483-2008, 2008.

Shephard, M. W., Cady-Pereira, K. E., Luo, M., Henze, D. K., Pinder, R. W., Walker, J. T., Rinsland, C. P., Bash, J. O., Zhu, L., Payne, V. H., and Clarisse, L.: TES ammonia retrieval strategy and global observations of the spatial and seasonal variability of ammonia, Atmos. Chem. Phys., 11, 10743–10763, doi:10.5194/acp-11-10743-2011, 2011.

Shephard, M. W. and Cady-Pereira, K. E.: Cross-track Infrared Sounder (CrIS) satellite observations of tropospheric ammonia, Atmos. Meas. Tech., 8, 1323–1336, doi:10.5194/amt-8-1323-2015, 2015.

Shephard, M. W., McLinden, C. A., Cady-Pereira, K. E., Luo, M., Moussa, S. G., Leithead, A., Liggio, J., Staebler, R. M., Akingunola, A., Makar, P., Lehr, P., Zhang, J., Henze, D. K., Millet, D. B., Bash, J. O., Zhu, L., Wells, K. C., Capps, S. L., Chaliyakunnel, S., Gordon, M., Hayden, K., Brook, J. R., Wolde, M., and Li, S.-M.: Tropospheric Emission Spectrometer (TES) satellite observations of ammonia, methanol, formic acid, and carbon monoxide over the Canadian oil sands: validation and model evaluation, Atmos. Meas. Tech., 8, 5189–5211, doi:10.5194/amt-8-5189-2015, 2015.

Slanina, J., ten Brink, H. M., Otjes, R. P., Even, A., Jongejan, P., Khlystov, A., Waijers-Ijpelaan, A., Hu, M., and Lu, Y.: Continuous analysis of nitrate and ammonium in aerosols by the Steam Jet Aerosol Collector (SJAC), Atmos. Environ., 35, 2319–2330, 2001.

Stremme, W., Ortega, I., and Grutter, M.: Using ground-based solar and lunar infrared spectroscopy to study the diurnal trend of carbon monoxide in the Mexico City boundary layer, Atmos. Chem. Phys., 9, 8061–8078, doi:10.5194/acp-9-8061-2009, 2009.

Stremme, W., Grutter, M., Rivera, C., Bezanilla, A., Garcia, A. R., Ortega, I., George, M., Clerbaux, C., Coheur, P.-F., Hurtmans, D., Hannigan, J. W., and Coffey, M. T.: Top-down estimation of carbon monoxide emissions from the Mexico Megacity based on FTIR measurements from ground and space, Atmos. Chem. Phys., 13, 1357–1376, doi:10.5194/acp-13-1357-2013, 2013.

Sun, K., Cady-Pereira, K., Miller, D. J. , Tao, L., Zondlo, M. A., Nowak, J. B., Neuman, J. A., Mikoviny, T., Müller, M., Wisthaler, A., Scarino, A. J., and Hostetler, C. A.: Validation of TES ammonia observations at the single pixel scale in the-

San Joaquin Valley during DISCOVER-AQ, J. Geophys. Res.-Atmos., 120, 5140–5154, doi:10.1002/2014JD022846, 2015.

Sutton, M. A., Reis, S., and Baker, S. (Eds.): Atmospheric ammonia: detecting emission changes and environmental impacts. Results of an expert workshop under the convention on long-range transboundary air pollution, Springer, New York, USA, 2009.

Sutton, M. A., Reis, S., Riddick, S. N., Dragosits, U., Nemitz, E., Theobald, M. R., Tang, Y. S., Braban, C. F., Vieno, M., Dore, A. J., Mitchell, R. F., Wanless, S., Daunt, F., Fowler, D., Blackall, T. D., Milford, C., Flechard, C. R., Loubet, B., Massad, R., Cellier, P., Personne, E., Coheur, P. F., Clarisse, L., Van Damme, M., Ngadi, Y., Clerbaux, C., Skjøth, C. A., Geels, C., Hertel, O., Wichink Kruit, R. J., Pinder, R. W., Bash, J. O., Walker, J. T., Simpson, D., Horváth, L., Misselbrook, T. H., Bleeker, A., Dentener, F., and de Vries, W.: Towards a climate-dependent paradigm of ammonia emission and deposition, Philos. T. R. Soc. Lond. B. , 368, 20130166, doi:10.1098/rstb.2013.0166, 2013.

Toon, G. C., Blavier, J.-F., Sen, B., Margitan, J. J., Webster, C. R., Max, R. D., Fahey, D. W., Gao, R., DelNegro, L., Proffitt, M., Elkins, J., Romashkin, P. A., Hurst, D. F., Oltmans, S., Atlas, E., Schauffler, S., Flocke, F., Bui, T. P., Stimpfle, R. M., Bonne, G. P., Voss, P. B., and Cohen, R. C.: Comparison of MkIV balloon and ER-2 aircraft measurements of atmospheric trace gases, J. Geophys. Res., 104, 26779–26790, 1999.

Van Damme, M., Clarisse, L., Heald, C. L., Hurtmans, D., Ngadi, Y., Clerbaux, C., Dolman, A. J., Erisman, J. W., and Coheur, P. F.: Global distributions, time series and error characterization of atmospheric ammonia (NH3) from IASI satellite observations, Atmos. Chem. Phys., 14, 2905–2922, doi:10.5194/acp-14-2905-2014, 2014a.

Van Damme, M., Wichink Kruit, R. J., Schaap, M., Clarisse, L., Clerbaux, C., Coheur, P.-F., Dammers, E., Dolman, A. J., and Erisman, J. W.: Evaluating 4 years of atmospheric ammonia (NH_3) over Europe using IASI satellite observations and LOTOS-EUROS model results, J. Geophys. Res.-Atmos., 119, 9549–9566, doi:10.1002/2014JD021911, 2014b.

Van Damme, M., Clarisse, L., Dammers, E., Liu, X., Nowak, J. B., Clerbaux, C., Flechard, C. R., Galy-Lacaux, C., Xu, W., Neuman, J. A., Tang, Y. S., Sutton, M. A., Erisman, J. W., and Coheur, P. F.: Towards validation of ammonia (NH_3) measurements from the IASI satellite, Atmos. Meas. Tech., 8, 1575–1591, doi:10.5194/amt-8-1575-2015, 2015a.

Van Damme, M., Erisman, J. W., Clarisse, L., Dammers, E., Whitburn, S., Clerbaux, C., Dolman, A. J., and Coheur, P.-F.: Worldwide spatiotemporal atmospheric ammonia (NH_3) columns variability revealed by satellite, Geophys. Res. Lett., 42, 8660–8668, doi:10.1002/2015GL065496, 2015b.

Velazco, V., Wood, S. W., Sinnhuber, M., Kramer, I., Jones, N. B., Kasai, Y., Notholt, J., Warneke, T., Blumenstock, T., Hase, F., Murcray, F. J., and Schrems, O.: Annual variation of strato-mesospheric carbon monoxide measured by ground-based Fourier transform infrared spectrometry, Atmos. Chem. Phys., 7, 1305–1312, doi:10.5194/acp-7-1305-2007, 2007.

Vigouroux, C., Hendrick, F., Stavrakou, T., Dils, B., De Smedt, I., Hermans, C., Merlaud, A., Scolas, F., Senten, C., Vanhaelewyn, G., Fally, S., Carleer, M., Metzger, J.-M., Müller, J.-F., Van Roozendael, M., and De Mazière, M.: Ground-based FTIR and MAX-DOAS observations of formaldehyde at Réunion Island and comparisons with satellite and model data, Atmos. Chem. Phys., 9, 9523–9544, doi:10.5194/acp-9-9523-2009, 2009.

von Bobrutzki, K., Braban, C. F., Famulari, D., Jones, S. K., Blackall, T., Smith, T. E. L., Blom, M., Coe, H., Gallagher, M., Ghalaieny, M., McGillen, M. R., Percival, C. J., Whitehead, J. D., Ellis, R., Murphy, J., Mohacsi, A., Pogany, A., Junninen, H., Rantanen, S., Sutton, M. A., and Nemitz, E.: Field inter-comparison of eleven atmospheric ammonia measurement techniques, Atmos. Meas. Tech., 3, 91–112, doi:10.5194/amt-3-91-2010, 2010.

Wagner, T., Beirle, S., Grzegorski, M., and Platt, U.: Global trends (1996–2003) of total column precipitable water observed by Global Ozone Monitoring Experiment (GOME) on ERS-2 and their relation to near-surface temperature, J. Geophys. Res.-Atmos., 111, 1–15, doi:10.1029/2005JD006523, 2006.

Whitburn, S., Van Damme, M., Kaiser, J. W., van der Werf, G. R., Turquety, S., Hurtmans, D., Clarisse, L., Clerbaux, C., and Coheur, P.-F.: Ammonia emissions in tropical biomass burning regions: Comparison between satellite-derived emissions and bottom-up fire inventories, Atmos. Environ., 121, 42–54, doi:10.1016/j.atmosenv.2015.03.015, 2015.

Wiacek, A., Taylor, J. R., Strong, K., Saari, R., Kerzenmacher, T. E., Jones, N. B., and Griffith, D. W. T.: Ground-Based Solar Absorption FTIR Spectroscopy: Characterization of Retrievals and First Results from a Novel Optical Design Instrument at a New NDACC Complementary Station, J. Atmos. Ocean. Tech., 24, 432–448, doi:10.1175/JTECH1962.1, 2007.

Wood, S. W.: Validation of version 5.20 ILAS HNO_3, CH_4, N_2O, O_3, and NO_2 using ground-based measurements at Arrival Heights and Kiruna, J. Geophys. Res., 107, 8208, doi:10.1029/2001JD000581, 2002.

Zhu, L., Henze, D. K., Cady-Pereira, K. E., Shephard, M. W., Luo, M., Pinder, R. W., Bash, J. O., and Jeong, G. R.: Constraining U.S. ammonia emissions using TES remote sensing observations and the GEOS-Chem adjoint model, J. Geophys. Res.-Atmos., 118, 3355–3368, doi:10.1002/jgrd.50166, 2013.